Chapter 2

Steam Oxidation of Fe-Based Materials

T. Dudziak

Additional information is available at the end of the chapter

http://dx.doi.org/10.5772/62935

Abstract

Coal-fired power units are important player in energy production worldwide; however, during combustion, solid fossil fuels produce large amount of CO_2 and contribute to climate change, to inverse this process, higher efficiency of power plants can be achieved through out higher steam parameters (higher T, higher p).

This chapter is related to steam oxidation at high temperatures where important aspects of degradation are discussed.

Steam oxidation in close-loop system using deionised water was used to perform research at high temperatures.

Analyses were performed at temperatures in the range of 600–750°C for 2000 h. Different steels were included during analysis, such as T22, T23, T91, T92, E1250, 316L, 347HFG, Super 304, 309S, 310S, and HR3C. Kinetic data, metal loss data, and microscopic investigations were performed in order to evaluate corrosion degradation of ferritic and austenitic steels.

Keywords: Steam oxidation, high temperature, coal power plants, metal loss, corrosion resistance, SEM, BSE, EDX, XRD

1. Introduction

Development of industry in the beginning of twentieth century is associated with combustion to produce heat and electric energy. The reserves of coal around the globe are massive, according to the US Energy Information Administration (EIA) coal reserves at 948×10^9 tons [1] are estimated; in contrast to gas or oil, coal is distributed more equally around the globe and is far cheaper, therefore more accessible for industry needs.

Although coal is more accessible than other fossil fuels; globally, the coal-burning process is responsible for high level of CO_2 emissions. It is report [2] that coal-fired electric power stations emit, on average, 1000 kg of CO_2 for every megawatt-hour [MWh] generated, which is more than twice the approximate amount of CO_2 released by a natural gas-fired electric plant, 550 kg of CO_2 per megawatt-hour [MWh] generated. Coal-fired power stations are one of the main CO_2 emitters and contributor to climate change. It is predicted that coal (hard coal or lignite) still stands as the main source of energy production in the next 20 years and will be responsible for even higher CO_2 emissions [3]. Moreover, energy production is predicted to grow yearly by 2.2% from 2008 to 2035 [4]. According to the International Energy Agency (IEA) energy statistics, electricity and heat production accounts for 41% of the total CO_2 emissions [5]. Conventional solid fossil fuel power plants contribute significantly to the global CO_2 emissions as discussed in the previous studies. The European Union (EU) has put restricted legislation in place in order to significantly reduce emissions from EU coal-fired power stations to 20% by the year 2020 in reference to the level in 1990 [6]. Recently, the observed significant changes in electric power sector related to reducing CO_2 emissions are strictly associated with ground-breaking development in material science and engineering. Throughout the last decades, tremendous progress has been achieved in the development of steels and technologies associated with energy production. Progress in steels performance for coal-fired power can be illustrated by the following numbers of outlet steam pressure and temperatures [7] leading to CO_2 decrease:

1. 1970s of the twentieth century: T = 538°C/538°C/16.7 MPa (167 bar),
2. 1980s of the twentieth century: T = 540°C/560°C/25.0 MPa (250 bar),
3. 1990s of the twentieth century: T = 560°C/580°C/27.0 MPa (270 bar),
4. Turn of the century twenty to twenty-first: T = 600°C/620°C/29.0 MPa (290 bar) USC,
5. In 2020 of the twenty-first century: T = 70°C/720°C/350 MPa (350 bar) AUSC.

Between 1970 and 2020, the outlet steam temperature increased approximately 150°C, whereas pressure reached as high as 350 bar in 2020 compared to 167 bar in 1970, showing the progress that has been achieved during the last 50–60 years. Among, the listed numbers, ultrasuper critical (USC) and advanced ultrasuper critical (AUSC) present the harshest conditions for structural steels, the steels facing high temperatures and pressures. The materials that were developed over 50–60 years ago are no longer currently suitable for USC and AUSC regimes due to poor corrosion resistance and inadequate high-temperature creep and strength properties. These technologies require austenitic steels and nickel (Ni)-based alloys with superior steam oxidation resistance. **Figure 2** shows creep strength versus temperature dependence for the most commonly used materials in coal-fired power sector.

Figure 1 further illustrates the correlation between efficiency and temperature in coal-fired power stations.

http://dx.doi.org/10.5772/62935

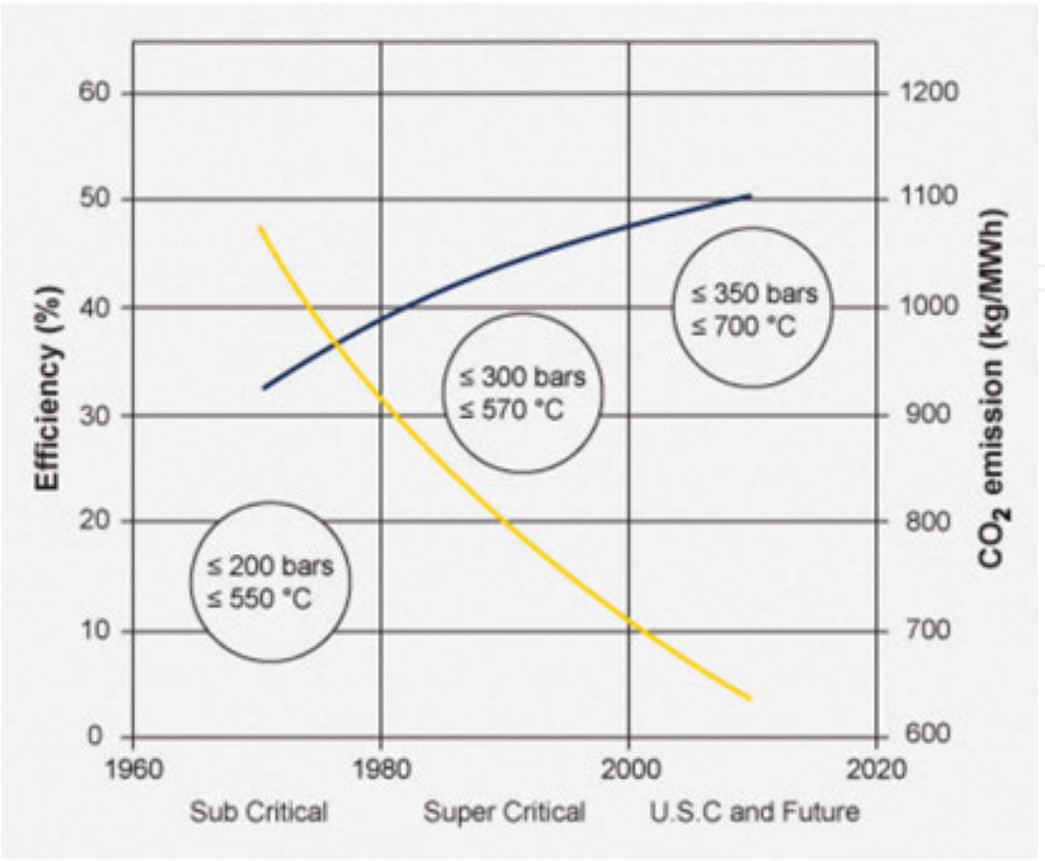

Figure 1. Effect of operating conditions on efficiency and emissions of steam power plants.

Development of materials for the energy sector, in terms of pressures and temperatures in superheaters (SH) and reheaters (RE) sections, is as follows [8]:

1. Ferritic steels: $p < 26$ MPa (260 bar), $T = 545°C$
2. Ferritic martensitic steels: $p = 26$ MPa (260 bar), $T = 545°C$
3. Austenitic steels: $p = 29$ MPa (290 bar), $T = 600°C$
4. Ni-based alloys: $p > 35$ MPa (350 bar), $T > 700°C$

Development of USC- and AUSC-based coal-fired power plants requires high-performance steels and Ni-based superalloys as shown in **Figures 1** and **2**. Reduction in CO_2 emissions from coal-fired power plants can be achieved by increasing the operating temperature (pressure) of water steam systems, which can give an increase in overall plant efficiency (**Figure 1**). Generally, 1% increase in absolute efficiency results in as much as 3% reduction in CO_2 emissions [9]. Hence, an increase in efficiency from 36 % (subcritical power stations) to 50–55% (USC and AUSC) leads to reduction of around 50% CO_2 emissions. Higher temperature means higher efficiency; however, higher corrosion rates occur in a steam atmosphere when ferritic, ferritic-martensitic, or medium Cr–Ni steels are used.

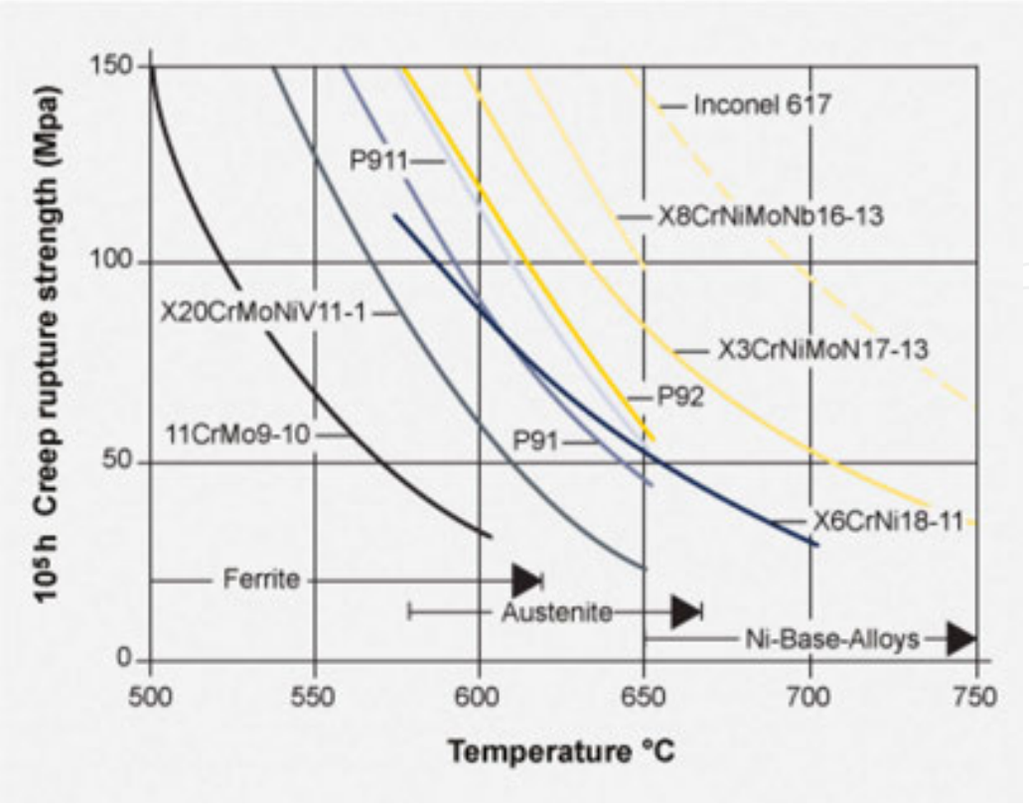

Figure 2. Materials for main steam pipes in power plants.

This chapter shows high-temperature steam corrosion degradation in the simplest way for the reader who wants to understand the fundamentals of corrosion phenomena at high temperatures.

2. Experimental procedure

2.1. Steam oxidation

Steam oxidation test rig, shown in **Figure 3**, was used to perform tests at high temperatures in a close loop [10]. Steam was generated by pumping highly purified deionised water from a reservoir placed underneath the furnace. In the furnace water, steam passes over the test samples and flows into a condenser before the water returns to the reservoir. The water used in the reservoir was double deionised.

The whole system was sealed using stainless steel flanges from both ends. Prior to steam oxidation test, the whole system was purged using oxygen-free nitrogen (OFN). Throughout the samples exposure period, this purge continues through the water reservoir in order to minimise the level of oxygen in the system. Prior to the high-temperature steam exposure, the furnace calibration was performed in order to place the materials in the middle of the hot zone. The calibration process ensured placement of the samples in the furnace at test temperature with an accuracy of ±5°C. Postexposed investigations of the samples covered the following:

macro and microexaminations using digital camera with macrolenses, environmental scanning electron microscope (ESEM) operating in backscatter electron mode (BSE) for better contrast, and a better phase designation. Finally, chemical analyses using energy X-ray-dispersive spectrometry (EDX) was employed to quantity examination of the corroded materials under steam conditions at elevated temperatures.

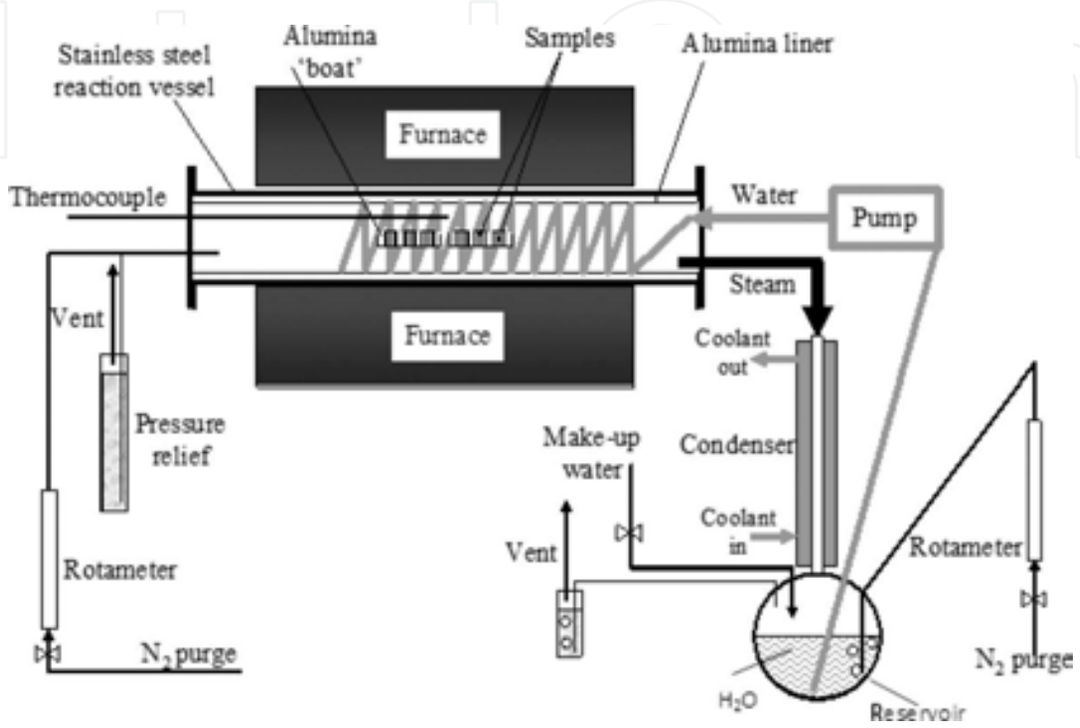

Figure 3. Steam oxidation rig used for the investigations of corrosion resistance in a steam atmosphere [10].

3. Materials

The materials, presented in the chapter, utilise most of the steels used in currently operating coal-fired power plants in Europe. Two main groups of the steels are distinguished as ferritic steels and austenitic steels. Ferritic steels represent the family of steels with adequate strength at high temperature up to 600°C (**Figure 1**), with relatively good corrosion resistance up to 500–550°C. The group possesses high coefficient of thermal conductivity (CTE), 50% higher than that met in more expensive austenitic steels. Furthermore, the ferritic steels show low coefficient of thermal expansion. The ferritic steels may contain high concentration of Cr, with the lack of Ni. The materials are mostly used in cooler areas of superheaters (SH) and reheaters and also in waterwalls in the temperature range where mild steels become too susceptible to creep. In general, the characteristic of ferritic steels can be shown as follows:

- Acceptable tensile strength (120 MPa) at temperatures up to 450°C
- Good creep properties at temperatures up to 550°C for 100,000 under 100 MPa

- Excellent weldability with no requirements for additional post-weld treatment (T22, T23 steels)
- Adequate steam oxidation up to 550°C

The family of ferritic steels can be divided further into several grades:

- GRADE 11 – P11/T11/13CrMo4 4
- GRADE 22 – P22/T22/10CrMo 9 10
- GRADE23 – P23/T23/HCM2S
- GRADE 24- T24/7CrMoVTiB10-10
- 1CrMoV

Austenitic steels are the family of materials with better corrosion-resistant properties with the addition of Ni and Cr to metal matrix. The steels are used in USC and A-USC coal-fired power plants in sections where materials cheaper than Ni-based alloys, with similar properties, are needed. The austenitic steels possess higher creep rapture strength at elevated temperatures than ferritic steels; nevertheless, the steels combine high CTE and poor coefficient of thermal expansion. The family was designed in order to increase the volume-strengthening precipitates fraction by replacing chromium carbides with more stable carbides, simultaneously freeing chromium to enhance corrosion resistance at elevated temperatures. The family of austenitic steels includes the following steels; AISI 302, 304, 321, 347, 316, 309, 310, ASME TP347HFG, Tempaloy A-1, Tempaloy A-3, Super304H, HR6W, NF709, and Esshete 1250 (E1250) The chemical composition of the steels reviewed in the chapter is listed in **Table 1**.

Material	Fe	Cr	C	Si	Mn	P	S	Al	Mo	V	Nb	Nb + Ta	W	Cu	B	Co	N	Ni
15Mo3	Bal.	-	0.16	0.35	0.60	≤0.035	≤0.035	-	0.30	-	-		-	-			-	-
T22	Bal.	2.25	0.10	0.25	0.45	0.0125	0.0125		1.00									
T23	Bal.	2.50	0.06	0.20	0.46	0.014	0.001		0.08	0.25	0.05		1.54		0.0023			0.14
T91	Bal.	8.36	0.10	0.12	0.45	0.003	0.009	0.022	0.90	-	-		-	0.017				
T92	Bal.	8.79	0.11	0.39	0.34	0.015	0.030	0.041	0.91	0.24	0.07		1.87					
E1250	Bal.	15.00	0.10	0.50	6.30	≤0.035	≤0.015	-	9.50	0.30	1.00		-	-	0.0050		-	9.50
316L	Bal.	16.60	≤0.003	0.60	1.80	≤0.040	≤0.030	-	2.10	-	-		-	-	-		-	11.00
347 HFG	Bal.	17.00	0.08	0.75	2.00	0.040	0.030		-	-	-		-	-	-		-	10.00
Super 304H	Bal.	18.40	0.10	0.20	0.80	0.045	0.030							3.00	-		0.1	8.80
HR3C	Bal.	25.00	0.06	0.40	1.20	-	-	-	-	-	0.45		-	-	-		-	20.00
309S	Bal.	23.00	0.08	0.75	2.00	0.045	0.03	-	-	-	-	-	-	-	-	-	-	14.00
310S	Bal.	25.00	0.20	1.50	2.00	0.045	0.03	-	-	-	-	-	-	-	-	-	-	21.00

Table 1. Chemical composition of steels currently in operation in coal-fired power plants.

http://dx.doi.org/10.5772/62935

4. Test results

4.1. Ferritic steels

Ferritic steels, such as 15Mo3, T22 and T23, under steam oxidation, have shown formation of nonprotective scale at temperatures higher than 600°C. The steels show lower values of operating temperature based on 100,000 h average stress rapture strength of 100 MPa than austenitic steels and Ni-based alloys. The formation of non-protective, thick scale is shown in **Figure 4** as an example of the T22 steel exposed at elevated temperatures, and higher temperature of the exposure as required was selected in order to present more clearly mechanism of ferritic steel degradation in a steam atmosphere.

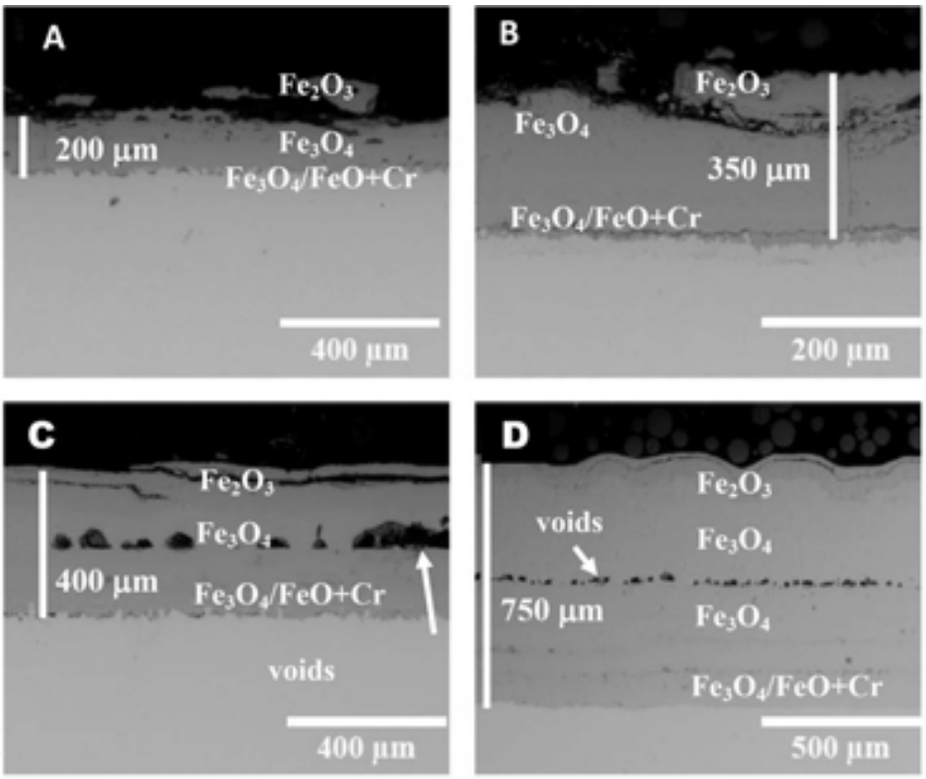

Figure 4. Cross-sectional image of T22 steel exposed in water steam at temperature: (A) 600°C, (B) 650°C, (C) 675°C, and (D) 700°C for 500 h (unpublished work, part of the project).

The T22 steel with ~2.25 wt% Cr under steam oxidation shows the formation of three oxides at high temperature [11]. The presented results indicate the formation of thick oxide scales consisting Fe_2O_3 (hematite), Fe_3O_4, (magnetite), and FeO (wustite). The formation of all three oxides is expected under steam oxidation conditions. Under 1 bar pressure, the oxygen partial pressure from the equilibrium dissociation of steam is high enough (two orders of magnitude higher) than the dissociation oxygen partial pressure required for Fe_2O_3 oxide [12]. Hence, development of thick scale is more than expected on steels belonging to ferritic family with GRADES 11, 22, 23, and 24. The Cr reservoir in such steels was not concentrated enough to

form thin protective scale. Ferritic steels with low concentration of Cr at temperatures above 580°C are covered predominantly with thick scales containing three types of oxides. Below 570–580°C formation of FeO is was not possible since the oxide is unstable. Hence, the steels exposed in steam environment below 580°C present much thinner oxide scale consisting Fe_2O_3 and Fe_3O_4 with diffused concentration of other elements such as Mn, S, and Cr. The total concentration of these elements rarely exceed 7 wt%. Voids were observed only at 675 and 725°C T22 steels, suggesting the highest rate of diffusion in both directions at these temperatures. The voids appear to be located at the original steam—substrate interface, suggesting two different mechanism of oxidise scale formations, the mechanism consider outward and inward diffusion of iron and oxygen ions, respectively. Some authors postulate that oxide scale on low ferritic steels grows by the outward diffusion of Fe [13], because Fe diffusion coefficient in iron oxides is much higher than that of oxygen [14]. Some authors, postulated, inward diffusion of oxygen, due to accelerate diffusion of oxygen throughout the grain boundaries [15]. The mechanism of voids formation has different variety that depends on author and scientific approach; in this chapter, the mechanism of void formation can be formulated in the following way: consider the diffusion couple between A (Fe_3O_4+Fe_2O_3 top layer) and B (Fe_3O_4+FeO+Cr bottom layer) in **Figure 4C** and **4D**, respectively. Both of these layers constitutes with different phases, showing different chemical potential, different ion flux, diffusion and number of defects giving different diffusion fluxes *J*. Since the diffusion fluxes are different, there will be a net flow, causing the couple to shift bodily. This can only occur if diffusion is by a vacancy mechanism between two layers (A and B). It should be noted that voids are formed at the original steam—substrate surface interface. Quadakkers et al. [16] showed that the voids formation can be observed on the ferritic oxide scale after long-term exposures that can be unevenly distributed or can coalesce to form a crack or a gap at the interface between the inner and outer layer. The formation of pores in the oxide scale may create significant consequences for mechanical and thermal properties. The low-alloyed ferritic steels developed thick oxide, originated from the phase structure and defects number within the crystallographic structure of the individual oxide. At temperatures above 570°C, FeO phase become stable under steam oxidising conditions; hence, oxide scale possesses three layers at temperatures above 570°C. For better clarity, and better understanding, **Figure 5** shows iron oxide phase stability at high temperatures [17].

The stability of FeO depends on two main factors, namely temperature and Cr concentration. The presence of FeO, in the oxide scale, dramatically accelerates thickness of the scale since the phase has higher Fe_3O_4 number of interstitial defects (support iron ion diffusion). Iron vacancies in FeO are responsible for the defects [18]; however, in Fe_3O_4, the main defects are localised in iron sublattice, neutral iron interstitials at low oxygen activity, and neutral iron vacancies at high oxygen activity. In Fe_2O_3, majority of the defects can be found in the oxygen sublattice than in iron sublattice. Generally, ferritic steels form multilayered scale [19], where predominantly Fe_3O_4 and FeO forms together with a thin layer of Fe_2O_3 can be observed. In steels with low Cr content, a thin layer enriched in Cr can be observed, some authors suggest formation of iron chromium spinel $FeCr_2O_4$ [20]. The findings are rather questionable since the concentration of Cr in the steels reaches 2–3 wt%, whereas development of iron-chromium spinel $FeCr_2O_4$ requires much higher concentration of Cr in bulk steel. Chemically, $FeCr_2O_4$

http://dx.doi.org/10.5772/62935

spinel should contains around 46 w% Cr, 25 wt% Fe, and 29 wt% O. The low-alloyed steels, due to low concentration of Cr in bulk steel, are unable to deliver through outward diffusion, showing that high concentration of Cr need for $FeCr_2O_4$ spinel development. In the case of low-alloyed steels, Cr-enrichment layer was formed with poor corrosion resistance. Formation of spinel as suggested by [11] should significantly decrease corrosion degradation because $FeCr_2O_4$ spinel possesses much lower number of defects, hence higher corrosion resistance than Fe_3O_4 and FeO phases. Similar to T22, the T23 steel with the addition of W, V, and Nb was introduced to achieve enhanced creep behaviour at higher temperatures [21] compared to T22 steel. In contrast to Lepingle et al. [22], it was found by T. Dudziak et al. [23] that the T23 steel showed a better corrosion resistance than that offered by the T22 steel. A slightly better corrosion resistance of the T23 in comparison with T22 can be related to W addition, when added, W through the chemical reaction with C, forms WC carbide:

$$W + C \rightarrow WC \tag{1}$$

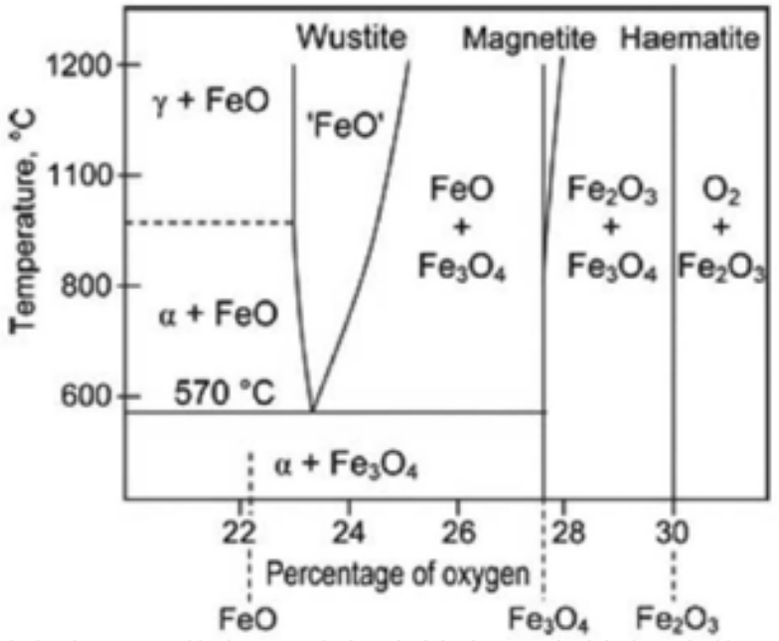

Figure 5. Iron-oxygen phase diagram [17].

Thus, due to the higher activity of Cr in T23, more Cr diffuses to the interface where enriched Cr layer or Fe_2CrO_4 spinel can form. However formation of $FeCr_2O_4$ spinel is rather unlikely to occur.

In contrast, in low-alloyed steels such as T22, Cr directly reacts with C to form carbides such as Cr_3C_2, Cr_7C_3 and $Cr_{23}C_6$ [24]. Hence, lower concentration of Cr in the bulk material, and lower activity of Cr, thus lower quantity of Cr diffuses to the surface, as a result thicker, with poor corrosion resistance oxide scale is forming. The comparison of T22 and T23 steels in terms of metal loss is shown in further part of this chapter. However, the results showed that T23

steel has a better corrosion resistance and lower metal loss at elevated temperatures. **Figure 4** shows scanning electron microscope (SEM) images in backscatter electron (BSE) mode of T22 and T23 steels exposed for 500 h at elevated temperatures. The images shown in **Figure 6** indicate distinct differences in thickness of the formed oxide scale.

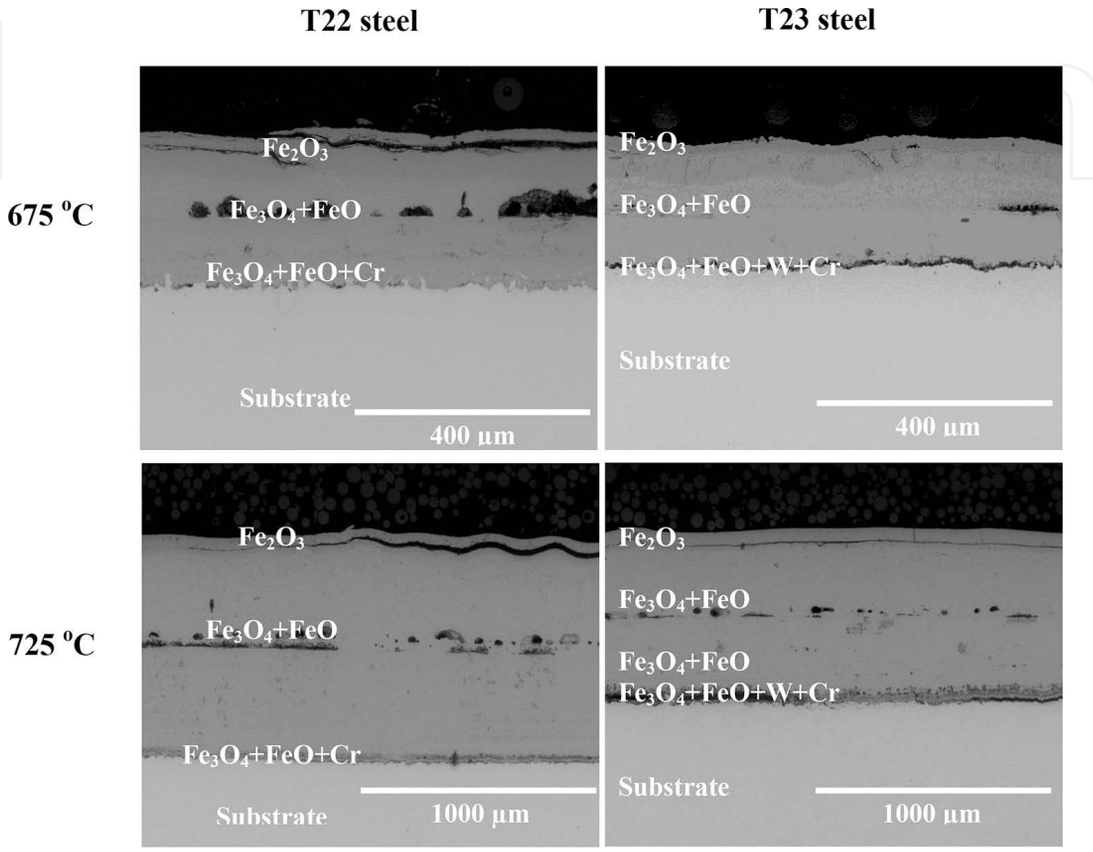

Figure 6. Comparison of oxide scale thickness between T22 and T23 ferritic steels exposed at 675°C and 725°C for 500 h.

4.2. Ferritic-martensitic steels

The steels with higher concentration of Cr in a matrix under high-temperature exposure in steam showed a better corrosion resistance. Similar to T23 in T92 steel, addition of W was introduced in order to enhance creep behaviour of T92 in relation to T91.

Because of a slightly higher concentration of Cr in ferrite matrix, the oxide morphologies in both steels are different compared to the low-alloyed steels. In general, the scale consists of different layers than that observed in the T22 and T23. Because T91 ferritic-martensitic steel showed a better corrosion resistance than that offered by T92 steel; in this chapter, the author mainly focuses on the T91 steel. Both steels were exposed at elevated temperatures:

1. T91 steel at T = 700, 750, and 800°C
2. T92 steel at T = 600, 650, 700, and finally 750°C.

In the T91 steel, the top part of the oxide scale was occupied mostly by Fe_3O_4 not by Fe_2O_3, some patches of Fe_2O_3 were observed, the inner layer consists thick band of Fe_3O_4 and the most inner layer consisted $(Fe,Cr)_3O_4$ spinel rich in Cr up to 11%. In terms of T92, the inner scale consisted $(Fe,Cr)_3O_4$ spinel with similar concentration of Cr as in the T91 steel. However, the presence of W at the oxide scale—the substrate interface was observed with concentration of W (varied from 2–5 wt%).

The findings in the T91 and T92 steels in relation to Cr content at the interface, the oxide scale—the substrate are in contradiction with the proposed values by Viswanathan et al. [25].

The author [25] proposed that steels with 9% Cr content should develop an enriched layer with as high as 45 wt% Cr at the oxide scale the substrate interface. However, in both 9 wt% Cr steels exposed at a steam atmosphere, concentration of Cr at the interface reached only about 13 wt% Cr.

The steel with 9 wt% Cr were exposed at temperatures higher than 570°C similar to the low-alloyed steels; therefore, high-temperature promoted development of FeO layer. On one hand, the formation of FeO is possible only at temperatures higher than 570°C, and upon the FeO phase, cooling may undergo eutectoid reaction forming mixture of Fe_3O_4 and Fe [26]. On the other hand, when the cooling process is high enough, FeO may be found at temperatures below 570°C. In addition to these, FeO may undergo oxidation to form Fe_3O_4 when oxidation is preceded under continuous cooling process.

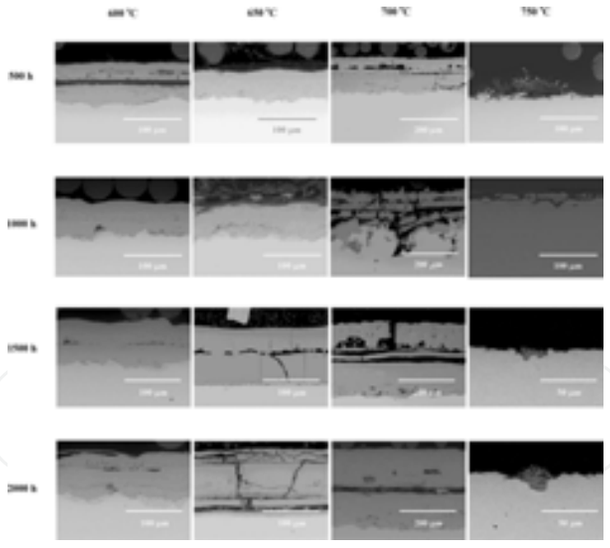

Figure 7. Cross-section images of ferritic martensitic T91 steel exposed in temperature range 600–750°C for 2000 h in a steam atmosphere.

Because diffusion of iron in FeO is extremely high, much higher than in Fe_3O_4, diffusion of oxygen and iron in Fe_2O_3 is extremely slow [27]. As a result, FeO possessed 90–95% of the total thickness of the oxide scale. However, this is a general remark, the percentage ratio can vary due to different external conditions; temperature, pressure etc. At higher temperature, above 570°C but below 650°C, the thickness of Fe_2O_3 and Fe_3O_4 layers increases. However, FeO is still

the major contributor in the oxide scale thickness. As mentioned, previously, FeO is unstable at temperatures below 570°C and starts to decompose.

In this study, formation of relatively thick Fe_3O_4 at temperatures 600–700°C was observed in T91, the results are shown in **Figure 7**. At higher temperature, the steels T91 and T92 show similar behaviour, where thin oxide scale developed after 500 and 1000 h of exposure, while after further exposure nodules formation were observed. The highest temperature of exposure show the development of nodules that possess two layered structure. The formation of nodules can be shown according to **Figure 8**. In the first stage of exposure in the steam oxidation atmosphere with high partial pressure of O, the steel with 9 wt% Cr develops thin protective $(Fe,Cr)_3O_4$ spinel scale. Since the concentration of Cr is limited to the formation of $(Fe,Cr)_3O_4$ spinel scale, no more Cr could outwardly diffuse from the metal matrix to sustain protective scale. In the same time, high activity of Fe ions, formed diffusion of Fe to the surface throughout spinel layer, showing the formation of nodule consisted high concentration of Fe. The formation of nodule is related to high flux of Fe ions that diffuses from the matrix and formed magnetite layer on the $(Fe,Cr)_3O_4$ spinel scale, as shown below. It was found that the amount of Fe_2O_3 on the surface was decreasing with increasing temperature; at 600°C, more Fe_2O_3 was found than at 750°C. Thus, the formation of Fe_3O_4 is more favourable at higher temperatures. These findings have been confirmed by Dudziak et al. [28].

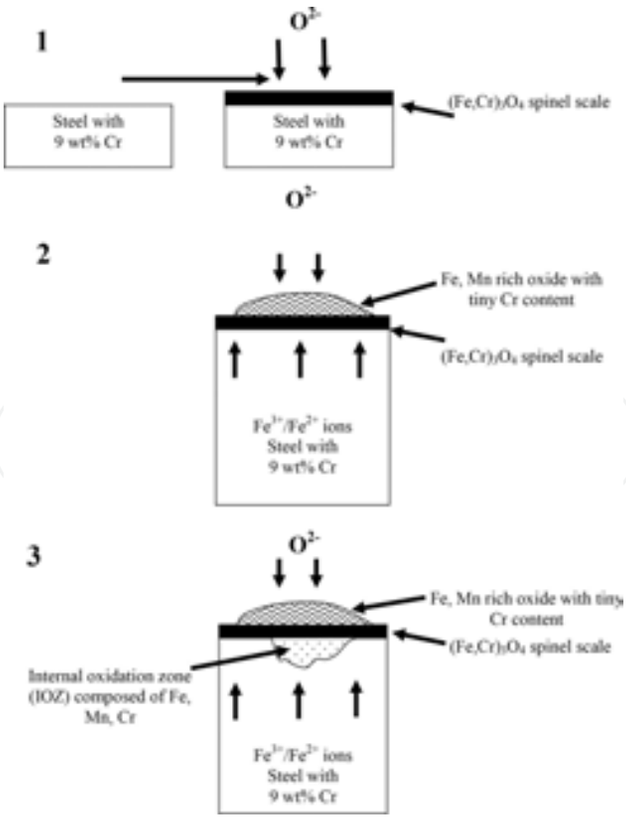

Figure 8. Development of nodule in 9 wt% Cr steel under the steam oxidation conditions.

The corrosion of 9 wt% Cr steels in a steam atmosphere obeys the formation of two-layered nodule, the nodule consists high concentration of Mn and Fe; 18 and 47 wt%, respectively, O content reaches 32 wt%, with Cr concentration equivalent to 3 wt%. The internal oxidation zone (IOZ), underneath the formed nodule, was observed after 1000 h exposure at 750°C. The IOZ consists of the mixture of Cr, Mn, and Fe oxides with variety of concentration.

It is believed that due to addition of W to the metal matrix, similar to T23 and T22, more free Cr can diffuse outwardly to the surface of the exposed material which indicates a higher Cr activity. This is due to the formation of WC (tungsten carbide) phase instead of Cr_3C_2, Cr_7C_3 and $Cr_{23}C_6$ phases. The higher Cr activity has a consequence in the formation of more protective $(Fe,Cr)_3O_4$ spinel scale, which is likely to occur in T92 compared to T91 steel. Metal loss data for T91 and T92 steels are shown in the last section of this chapter.

4.3. Austenitic steels

This subchapter provides information regarding austenitic steels with Cr concentration higher than 10 wt% Cr in the metal matrix. The steels (with 12 and 16 wt% Cr) in the matrix were tested in the same conditions as the low-alloyed and 9 wt% Cr steels. **Figure 9** shows cross section images in BSE mode for E1250 and 316L steels. The E1250 steel showed development thin, protective but extremely brittle oxide scale. Under the steam oxidation conditions, the scale showed lack of adherence at the peak of concave geometry. The behaviour is related to tensile and shrink stresses upon heating and cooling from high temperature to room temperature. Furthermore, delamination and poor adherence is related to the formation of a very thin oxide scale. A thin oxide scale with lack of plasticity and lack of relaxation energy could not consume stresses released upon heat treatment. Finally, delimitation of the oxide scale was found on the surface with the highest inclination angle. It can be concluded that exfoliation of the formed oxide scale can be invoked by different coefficient of thermal expansion (CTE), while CTE depends directly from chemical composition and microstructure.

The brittleness of the formed oxide increases with time of exposure and temperature; in contrast to E1250 steel, the 316L with 16 wt% Cr indicated the formation of a thin, protective and adherent oxide scale under the steam oxidation conditions at 700–800°C. The E1250 steel showed formation of a thick scale at 800°C, indicating limited usability of the steel in a steam atmosphere. Such behaviour indicates that concentration of 12 wt% Cr is suitable for conditions where steam temperature reaches lower values below the range 750–800°C. Above this temperature, acceleration in thickness of the oxide is observed.

The presented results, in **Figure 9**, clearly demonstrates, that 16 wt% Cr steel has shown significantly better corrosion resistance in steam environment at temperature as high as 800°C. The scale consisted a single oxide layer; however, a thick layer varies with composition; the top part of the oxide scale consist 7 wt% Cr, 5 wt% Mn, 4.5 wt% Ni, and 57 wt% Fe, respectively. The bottom part of the oxide scale was rich in Cr with 14 wt%, and relatively low content of Mn (3 wt%), high Ni concentration (20 wt%), and rich Fe content equivalent to 43 wt%.

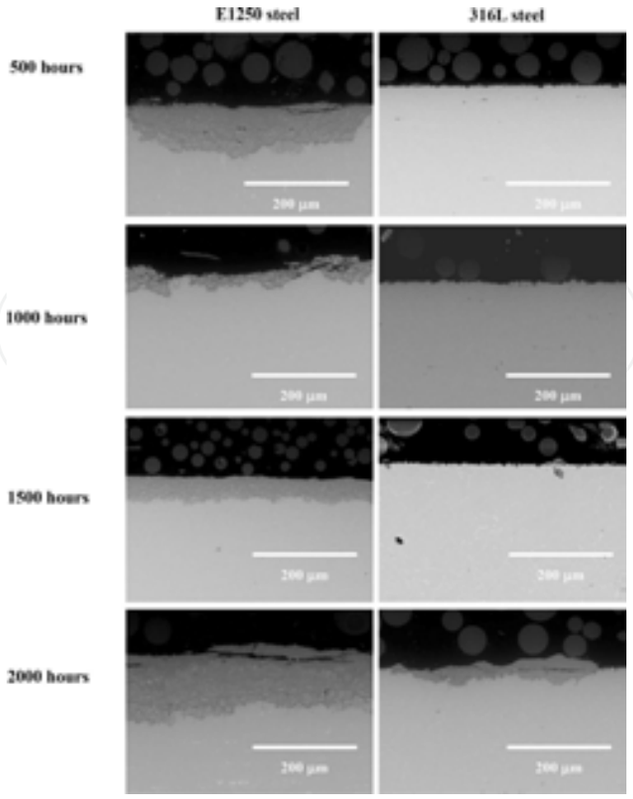

Figure 9. Cross-sectioned images performed via SEM in BSE mode of two austenitic steels with 12 wt% Cr E1250 and 16 wt% Cr 316L steels exposed at 800°C for 2000 h in a steam atmosphere.

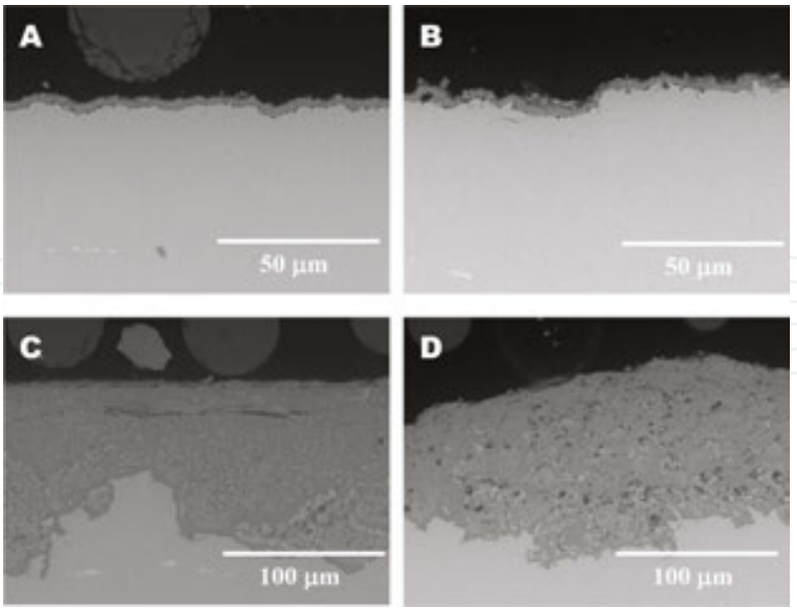

Figure 10. Cross-sectioned images performed via SEM in BSE mode of two austenitic steels with (A, C) 17 wt% Cr and (B, D) 18 wt% Cr steel exposed at 800°C for 2000 h in a steam atmosphere.

Alternatively, the steel with 16 wt% Cr manifests the formation of a thin, protective oxide scale rich in Cr (36 wt% Cr, 30 wt% Fe, 6 wt% Ni, and 2 wt% Mo) suggesting the formation of $(Fe,Cr)_3O_4$ spinel with the incorporation of additional elements. However, long exposure of 16 wt% Cr steel at high temperature indicated the likelihood of the formation of nodules. The nodules with double-layered structure were found; the external part of nodule consisted high concentration of Fe (60 wt%), relatively low Cr and Ni content (9 and 4 wt%). Internal part of nodule consisted much higher Cr concentration (20 wt%) and higher Ni content (20 wt%). Nevertheless, nodules were distributed randomly in 16 wt% Cr steel compared with 12 wt% Cr steel showing a better corrosion resistance.

The cross-sectioned microstructures of 17 wt% Cr (TP347HFG) and 18 wt% Cr (Super 304) are shown in **Figure 10**. In comparison to E1250 and 316L austenitic steels showed better performance in a steam atmosphere. The steels were exposed in the same conditions using the same test rig presented in **Figure 3**. The steels with 17 and 18 wt% Cr were exposed only at 800°C. The steels showed similar behaviour in steam conditions; however, better corrosion resistance than the materials with lower Cr content.

The oxide scale formed on the exposed materials showed thickness in the range of 2–5 μm, and the scale of 347HFG consists of high levels of Cr, Fe, and oxygen with concentration of 19, 47, and 25, respectively, indicating formation of Fe-Cr spinel. Concentration of Ni in the top part of the oxide scale showed value close to 6 wt%. Relatively high concentration of Ni found in the top layer suggests the formation of porous oxide scale under the steam oxidation conditions. Saunders et al. [29] reported that steels exposed in a steam atmosphere in general, promotes the formation of a more porous scale. This is related to an increase in cation diffusion and consequent vacancy condensation, thereby developing a porous structure. Enriched layer of Cr was found in the oxide scale—the substrate interface where concentration reached 33 wt %, with a tiny amount of Mn (2.9 wt%) and Ni (6.4 wt%). In comparison, the steel with 18 wt % showed rich in Cr oxide scale with concentration of 33 wt%, 30 wt% Fe, 3.3 wt% Ni, and 2.2 wt% Cu. Copper addition stabilise austenite structure, hence, improve outward Cr diffusion, presenting the formation of enriched Cr oxide scale in comparison to 347HFG steel. Both steels formed the oxide scale with good adherence, spallation was observed under the steam oxidation conditions.

Highly alloyed steels, such as 309S, 310S, HR3C, are used in coal-fired power plant industry for the hottest sections of superheaters (SH) and reheaters (RH). The steels were tested under scientific grant funded from the National Science Centre in Poland. Grant number: 2014/13/D/ST8/03256, entitled:

> *Development mechanism of thermodynamically stable, thin and protective oxide scales formation at high temperatures in pure water steam on the material based on Fe and Ni structures with high chromium content*.

The steels with Cr content higher than 20 wt% Cr were exposed for 2000 h at 800°C. The steels HR3C, 309S, 310S were tested in the same the steam oxidation rig, presented in **Figure 3**. The steam oxidation tests were performed for 2000 h in the rig presented in **Figure 3**, kinetic data were obtained via standard weight method, and kinetic results are shown in **Figure 11**.

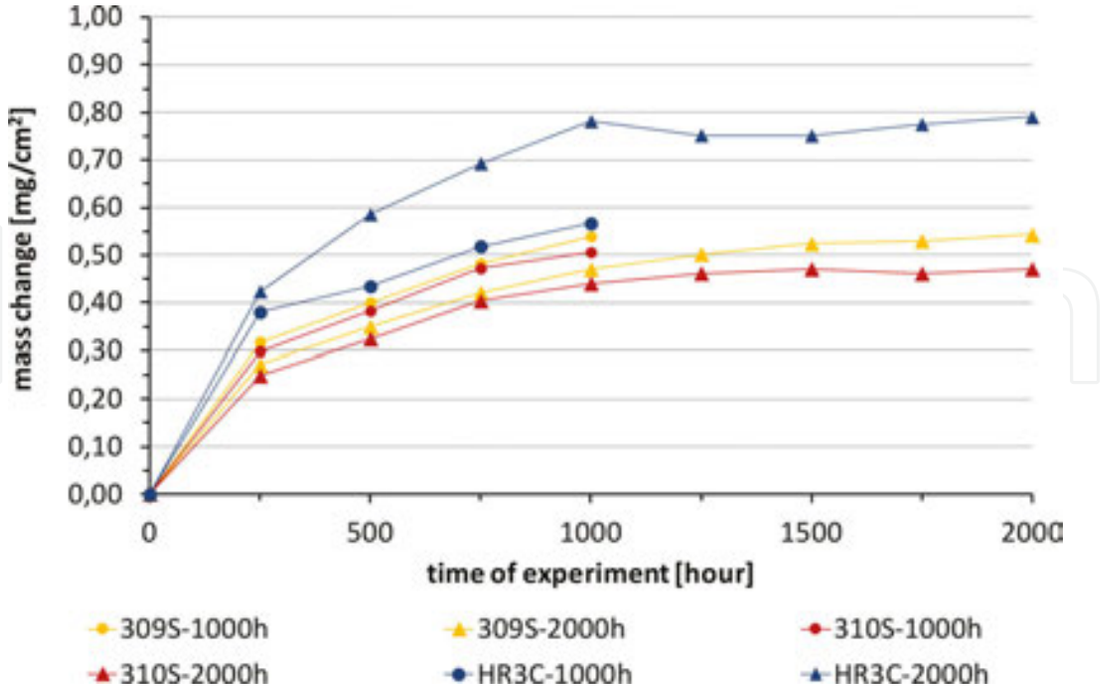

Figure 11. Kinetic data for 309S, 310S, and HR3C steels exposed to the steam oxidation regime at 800°C for 2000 h.

The steels showed a relatively low mass gain at 800°C. All the exposed materials showed similar mass change with difference of 0.05 mg/cm^2 after 2000 h of exposure, suggesting the same mechanism of corrosion behaviour. The highest mass gain was achieved for HR3C and the lowest for 310S steel even if the difference was not significant. The surface microstructures of highly alloyed steels exposed to steam conditions are shown in **Figure 12**. Chemically, 310S steel shows development of the oxide rich in Mn, Cr, and O with composition of 45, 22, 30 wt %, respectively, and some areas of the 310S steel surface was enriched in Mn with concentration of 50 and 40 wt%.

In general, in the steel 309S, developed morphology with high content of Mn, Cr, and Si oxide, some areas are enriched with Mn, O, and Fe with composition of 38, 19, 32 wt%, respectively. Therefore, both steels 310S and 309S developed similar morphologies under the steam oxidation, no cracks, spallation and other sign of corrosion degradation on the surface was observed, suggesting high adhesion of the oxide scale to the metallic substrate.

The HR3C showed similar surface structure as 309S and 310S, where rich in Cr, Mn and O phase developed, presenting appropriate corrosion performance at elevated temperature. The results shown here are in contrast with other findings that reports the minimum content of Cr promoting the formation of stable Cr_2O_3 in steam requires 20–25 wt%., Wasilewski, Robb, Giggins, and Pettit [30, 31]. On the other, the study performed by Birks and Rickret [32] suggests that if Cr reaches 10 wt%, then spinel $(Cr,Me)_3O_4$ should develop containing some quantity of Fe, Mn, Mo (alloying elements), the authors suggested that for the formation of thin, adherent, protective Cr_2O_3 20 wt% Cr is requires 20 wt% or more.

http://dx.doi.org/10.5772/62935

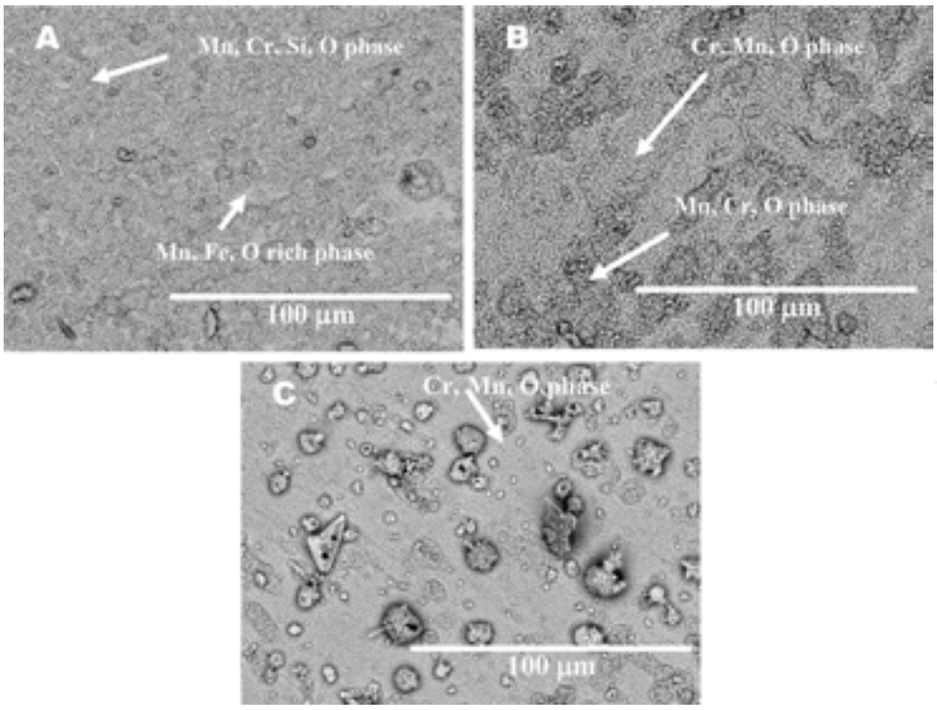

Figure 12. Surface morphologies of: (A) 309S, (B) 310S, (C) HR3C after exposure at 800°C for 2000 h in a steam atmosphere.

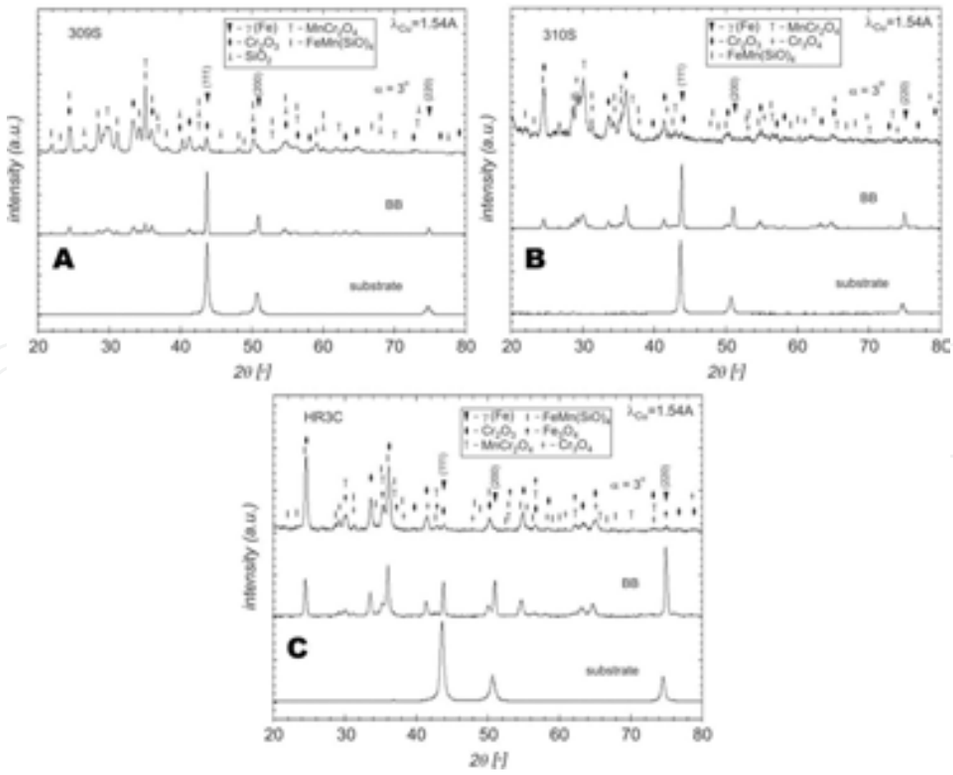

Figure 13. XRD pattern of (A) 309S, (B) 310S, (C) HR3C after exposure at 800°C for 2000 h in a steam atmosphere.

The current study shows that in a steam atmosphere, concentration of 23–25 wt% Cr is unable to promote the formation of pure Cr_2O_3, whenever highly alloyed steel is exposed at high temperatures, the formed oxide scale (Cr_2O_3) contain alloying elements, diffused from the bulk steel. Hence, it is impossible to develop Cr_2O_3 exclusively when the steel contains 20 wt% or even more Cr. The study shows that under 800°C, element activity, chemical potential, diffusion coefficient of Mn, Fe, Si are high enough to contribute in the scale formation; therefore, always some quantity of alloying elements will be observed, and hence the formation of exclusively pure Cr_2O_3 should be treated more as myth than the real finding.

In order to confirm the findings, **Figure 13A–C** shows XRD patterns for highly alloyed steels under the steam oxidation conditions.

5. Metal loss of steels in steam atmosphere

Following the steam oxidation exposures at high temperatures, the exposed samples were cold mounted to protect the potentially delicate oxide scale. The polished cross sections were measured using an image analyser to generate accurate measurements of the amount of metal remaining after the steam oxidation tests. **Figure 14** shows a schematic on the *x*-*y* stage for the analysis.

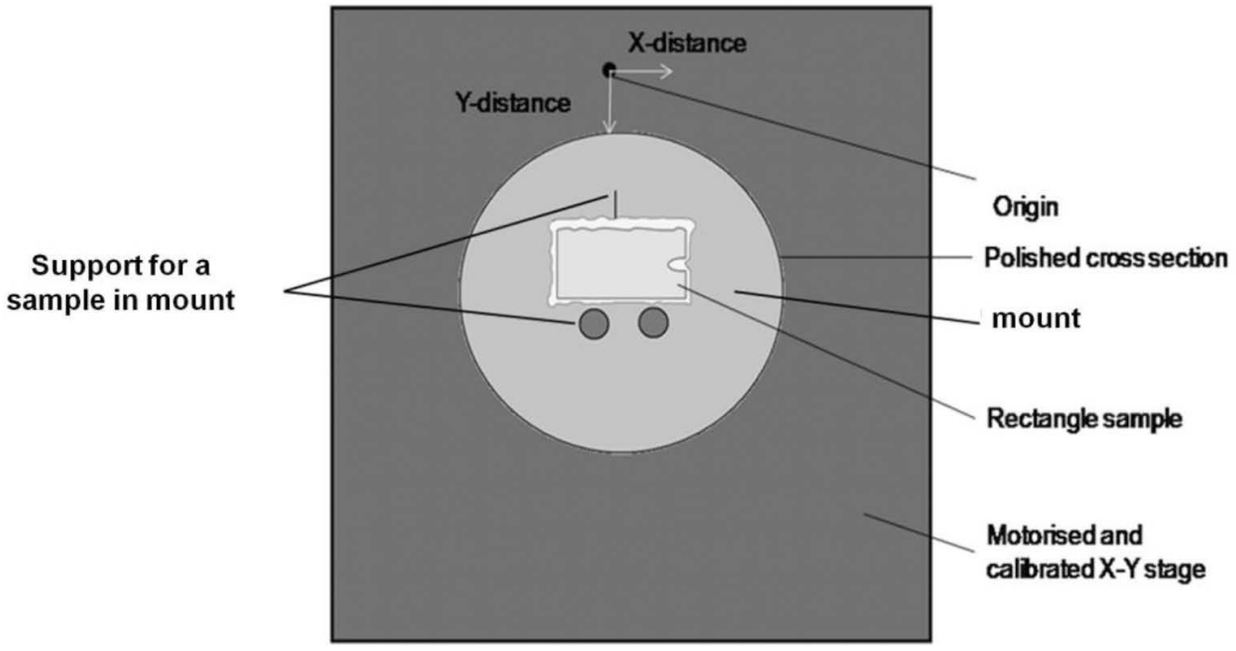

Figure 14. Schematic of a rectangular samples cross-section on the digital image analyser stage.

The best results of metal loss analyses were assessed when ~55 or more points around the sample was captured. The images were recorded during measurement and stitched together. The obvious metal losses in each of these images were pinpointed. **Figure 15** demonstrates the function of image analyser (e.g., at point B the *x* value = *b*2 and the *y* value = *a*2).

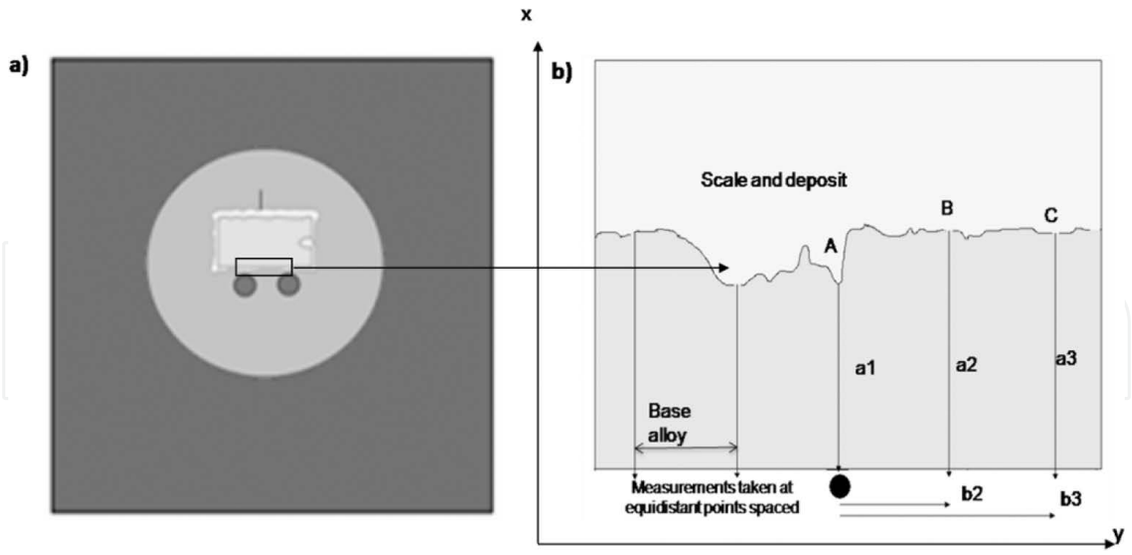

Figure 15. Illustration of function of image analyser (a) stage and sample; (b) determining metal loss from the images recorded.

Figure 16A–D compares metal loss between ferritic steels with low Cr content, whereas metal loss data for ferritic martensitic, and mid alloyed steels exposed to the steam oxidation environment is shown in **Figure 17** compares metal loss between ferritic, ferritic martensitic, and highly alloyed steels exposed to the steam oxidation environment. It was found that the steel with W addition presented lower metal loss compared to the T22. Therefore, it is confirmed that addition of small quantity of W improves high-temperature corrosion resistance. Metal loss of ferritic-martensitic steel reveals reverse situation, the steel with W addition shown a slightly higher metal loss than that offered by T91 steel. However, these findings are in good agreement with the published data [10]. The steel with 12 wt% Cr showed much higher metal loss than that observed in 16 wt% Cr steel, whereas a lower loss was observed in the low-alloyed steels and ferritic martensitic steels under the steam oxidation conditions. Furthermore, the steel with 12 wt% showed a higher spread in terms of metal loss calculations; the lowest metal loss data was achieved at 700 and 750°C for 2000 h of exposure where metal loss reached 80 μm. At the highest temperature, the metal loss value doubled. The steel with 16 wt% Cr showed as little as 15-μm value of metal loss in temperature range 700–800°C after 2000 h of exposure. The steel with 16 wt% Cr (316L) indicated much better corrosion resistance in a steam atmosphere than that offered by E1250 steel (12 wt% Cr). The calculated values of the metal loss, showed narrower data set as shown in the 12 wt% Cr steel. The behaviour suggests much better corrosion resistance at an elevated temperature. Furthermore, the majority of the metal loss results are accumulated in blue region indicating via thin blue stripe in **Figure 16D**. The calculations for 12 wt% Cr steel were not performed for 500–1500 h at 700 and 750°C, respectively, due to metal loss lower than 5 μm in terms of cumulative probability [%]. The values lower than 5 μm are hard to evaluate furthermore such calculations are cursed with high error probability. Similarly, metal loss calculations for 347HFG, 309S, 310S, and HR3C were not estimated due to the metal loss value lower than 5 μm.

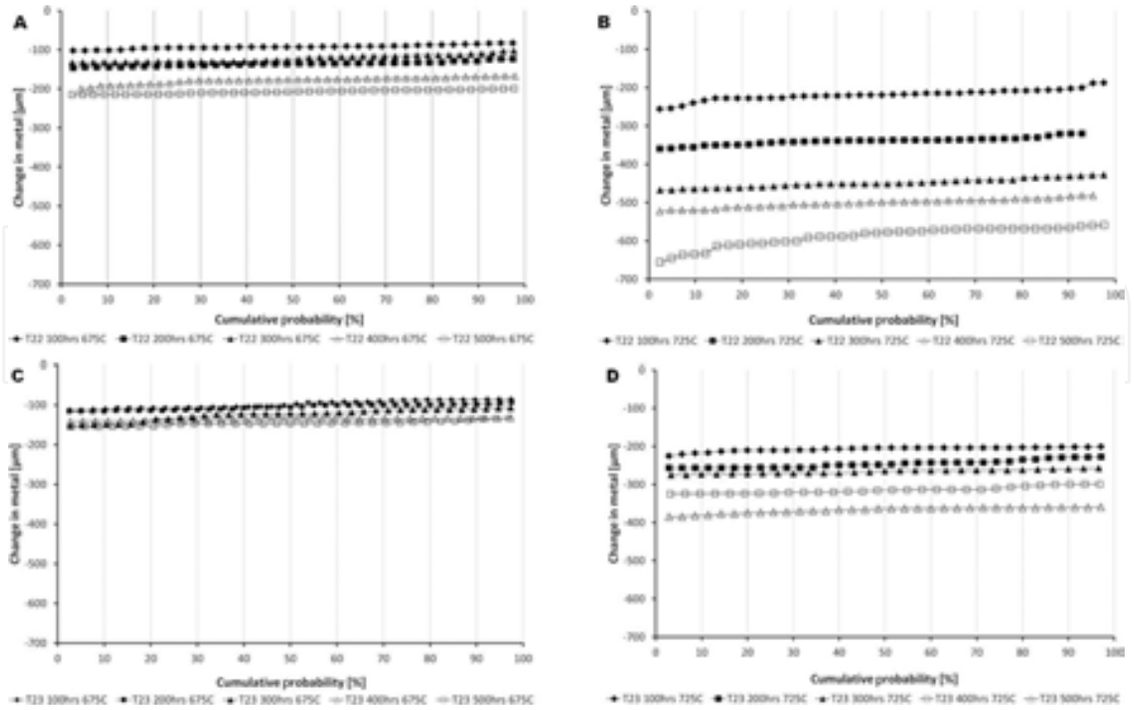

Figure 16. Metal versus metal loss data of T22 (A, B) and T23 ferritic steel (C and D) after exposure at 675 and 725°C in a steam atmosphere.

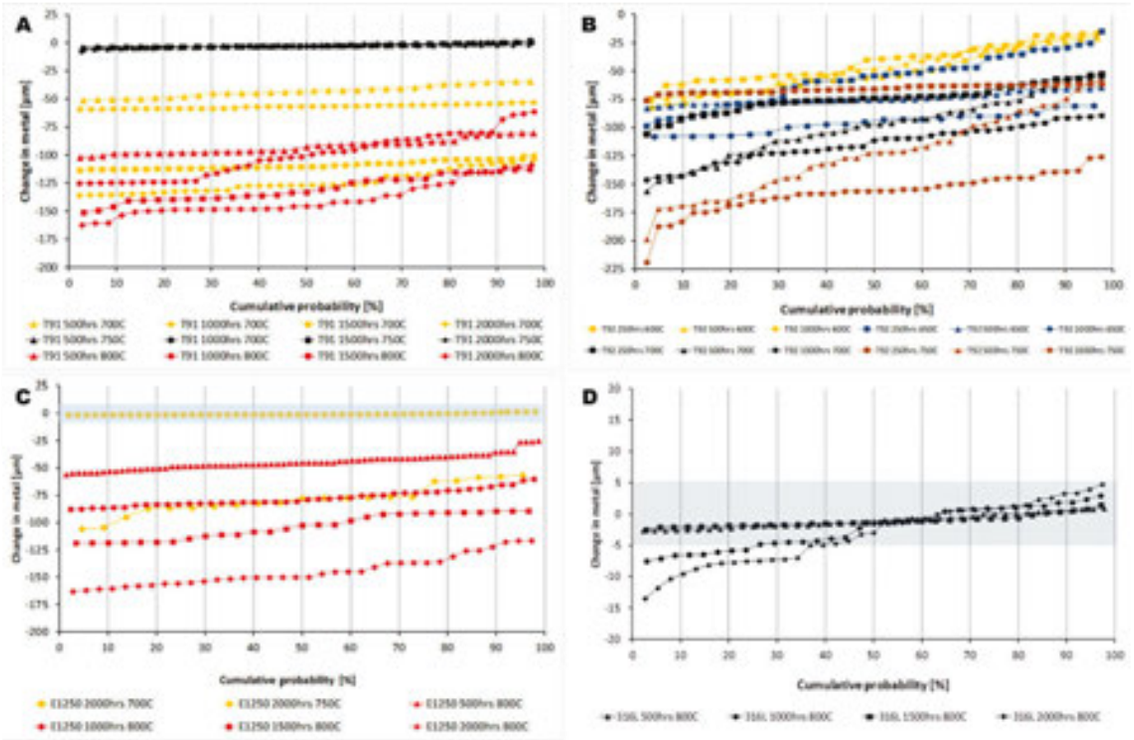

Figure 17. Metal loss data (A) T91, (B) T92, (C) E1250, and (D) 316L steels at elevated temperatures exposed in a steam atmosphere.

http://dx.doi.org/10.5772/62935

6. Conclusions

The aim of this chapter was to present the latest results of the steam oxidation work performed in unique close-loop system under high temperatures. In this study, nine steels with different chemical compositions were exposed. The steels represent ferritic, ferritic-martensitic, and austenitic grades. The tests were carried out in close loop and the steam oxidation system at different temperatures ranging 600–800°C. Based on the results, the following conclusions are drawn and it can be concluded that ferritic steels such as T22 and T23 form thick oxide scales, indicating the formation of all three Fe-based oxides at temperatures above 570°C. The oxide scales above 650°C show voids formation between two Fe_2O_3 and Fe_3O_4 layers in ferritic materials; however, addition of small portion of W (up to 3 wt%) to T23 steel delivers enhancement in corrosion and resistance in pure a steam atmosphere compared to T22 steel. Calculated metal loss for ferritic steel reached almost 650 μm at 725°C. Nevertheless, the formed oxide scale show good adherence to the substrate, and lack spallation was observed. The steel with 9 wt % Cr T91, T92 in comparison to T22, T23 steels showed a slightly better corrosion resistance as expected. However, at 750°C, "bell shape" temperature dependence in ferritic martensitic steels was found. Finally, addition of small portion of W to 9 wt% Cr steel showed adverse effect than that found in 3 wt% Cr steel (T22). The steel with 12 wt% Cr (E1250) showed formation of flaky, poor adherent scale, and the scale spallation was observed mainly for concave geometry; however, much lower mass gain was observed than that found in ferritic steels. The steel with higher content of Cr (16 wt% Cr, 316L steel) showed better corrosion resistance than that offered by 12 wt% Cr steel; however, at 800°C, test for 2000 h of exposure accelerated degradation was observed due to rich Fe nodule formation. The steels with 17 and 18 wt% Cr showed again better corrosion resistance than that offered by 12 and 16 wt% Cr steel; lower number of nodules and chromium-rich oxide was found on the surface in 18 wt% Cr steel. In comparison to ferritic steels, metal loss calculation in austenitic steels showed that only steel with 12 wt% Cr indicates more than 5 μm metal loss, whereas other materials showed metal loss lesser than 5 μm, even after 2000 h of exposure. High-alloyed steels, such as HR3C, (25 wt% Cr) 310S, 309S (>22 wt% Cr), showed the formation of protective scales and Cr_2O_3, Cr_3O_4, $MnCr_2O_4$ phases, and lack of spallation occurred.

Author details

T. Dudziak

Address all correspondence to: tomasz.dudziak@iod.krakow.pl

Foundry Research Institute, Centre for High Temperature Studies, Zakopiańska, Kraków, Poland

References

[1] EIA International Energy Statistics. Coal: Recoverable Reserves, (2012)

[2] How much carbon dioxide is produced when different fuels are burned? US EIA

[3] S. J. Davis, R. H. Socolow, Commitment accounting of CO2 emissions, Environmental Research Letters, 9 (8), (2014)

[4] Annual Energy Outlook 2010 with Projections to 2035, Department of Energy DOE/EIA-0383 (2010)

[5] International Energy Agency (IEA), Energy Efficiency Indicators for Public Electricity Production from Fossil Fuels, IEA Information paper (2008)

[6] I. Traynor and D. Gow, EU promises 20% reduction in carbon emissions by 2020, The Guardian Newspaper (2007)

[7] T. U. Kern, K. Weighthardt, H. Kirchner, Material and design solutions for advanced steam power plants Proceedings of the Fourth International Conference on Advances in Materials Technology for Fossil Power Plants. Hilton Head Island, USA (2004)

[8] I. Wright, R. Dooley, A review of the oxidation behaviour of structural alloys in steam, Oak Ridge National Laboratory, Institute of Materials, Minerals and Mining and ASM International, Published by Maney for the Institute and ASM International (2010)

[9] J. Henry, G. Zhou, T. Ward, Lessons from the past: materials-related issues in an ultra-supercritical boiler at Eddystone plant, Materials at High Temperatures, 24 (2007), 249-258

[10] M. Lukaszewicz, N. J. Simms, T. Dudziak, J. R. Nicholls, Effect of steam flow rate and sample orientation on steam oxidation of ferritic and austenitic steels at 650 and 700°C, Oxidation of Metals, 79(5-6), (2013), 473-483

[11] T. Dudziak, High temperature performance of materials for the energy sector exposed to water steam, Transactions of Foundry Research Institute, 54(3), (2014), 43-58.

[12] Program on Technology Innovation: Oxide Growth and Exfoliation on Alloys Exposed to Steam, Electric Power Research Institute (EPRI), Final Report, (2007)

[13] G. Granaud, R. A. Rapp, Thickness of the oxide layers formed during the oxidation of iron. Oxidation of Metals. 1977; 11:193-198

[14] Reddy KPR, Cooper AR. Oxygen diffusion in MgO and a-Fe2O3. Journal of the American Ceramic Society. 66, (1983);664-666

[15] W. Wegener, G. Borchardt, Analysis of oxygen-18 tracer profiles in two-stage oxidation experiments (I): predominant oxygen diffusion in the growing scale. Oxidation of Metals, 36, (1991), 339-357

[16] W. Quadakkers, Mechanisms of steam oxidation in high strength martensitic steels, International Journal of Pressure Vessels and Piping. 84 (2007), 75

[17] Jei-Pil Wangc, Dong-Won Lee, Jung-Yeul Yun, Shun-Myung Shina, In-Soo Kim, Study on the Reduction of Forging Oxide Scale using Hydrogen, Journal of Korean Powder Metallurgy Institute 20(3), (2012), 174-179

[18] Y. Limoge, J. L. Bocquet, Self diffusion and point defects in iron oxides: FeO, Fe3O4, a-Fe2O3, Defects and Diffusion Forum, 194-199, (2001), 1051-1056

[19] S. R. Paterson, R. S. Moser and T. W. Rettig, "Interaction of Iron Based Materials with Water and Steam - Oxidation of Boiler Tubing", 1992 Paper 8.

[20] A Fry, S Osgerby, M Wright, Oxidation of Alloys in Steam Environments - A Review, National Physical Laboratory, (NPL) Report NPL Materials Centre (2002)

[21] K. Rodak, A. Hernas, A. Kielbus, Characteristics of new low-alloy steel T23 for power industry, 10th Jubilee International Scientific Conference, Achievements in Mechanical and Materials Engineering, Conference Proceedings, 483-486

[22] V. Lepingle, G. Louis, D. Petelot, B. Lefebvre and J.C. Vaillant, "High Temperature Corrosion Behaviour of Some Boiler Steels in Pure Water Vapour." High Temperature Corrosion and Protection of Materials 5, Materials Science Forum, 369-372, Trans Tech Publications, Switzerland, (2001), 239-246

[23] T. Dudziak, S. Grobauer, N. Simms, U. Krupp, M. Lukaszewicz, Metal loss of steam-oxidized alloys after exposures at 675°C and 725°C for 500 hours, High Temperature Materials and Processes, (2015), 1-16

[24] J. Ellis,M. Haw, Chromium Carbides, Materials World 5 (11):1(1997), 36

[25] R. Viswanathan, J. Server, R. Viswanathan, J. Server, Boiler materials for USC coal power plants-streamside oxidation, Journal of Materials Engineering and Performance, (2006), 15, 225-274.

[26] R. Chen, W. Yuen, Oxide-scale structures formed on commercial hot rolled steel strip and their formation mechanisms, Oxidation of Metals, 56, (2001), 89-118.

[27] F. Gesmundo, F. Viani, The formation of multilayer scales in the parabolic oxidation of pure metals: II Temperature and pressure dependence of the different rate constants, Corrosion Science, (1978), 18, 231-243.

[28] T. Dudziak, M. Lukaszewicz, N. Simms, J. Nicholls, Analysis of high temperature steam oxidation of superheater steels used in coal fired boilers, Oxidation of Metals, (2015), 1-17, DOI 10.1007/s11085-015-9593-9.

[29] S.R.J. Saunders 1, M. Monteiro, F. Rizzo, The oxidation behaviour of metals and alloys at high temperatures in atmospheres containing water vapour: A review Progress in Materials Science 53 (2008) 775-837

[30] G. E. Wasielewski, R. A. Rapp, High Temperature Oxidation, in "The Superalloys", edited by C.S. Sims and W. Hagel, John Wiley & Sons, Inc., (1972), 287-317.

[31] G. S. Giggins, F. S. Pettit, Oxidation of Ni-Cr-Al alloys between 1000 and 1200 oC, Journal Electrochemical Society, 118, (1971), 1782.

[32] N. Birks, H. Rickert, Development of scales in oxidation conditions in 30, 60, 80 wt% Cr Ni-Cr alloys, Journal of the Institute of Metals, 91, (1962-1963), 308.

IntechOpen